**Abstract** This paper investigates the singular optics of non-paraxial light beams in the near field when the light behaves as a tractor beam. New insights into the optical pulling force, which is usually represented by integrating the stress tensor at a black box enclosing the object, are interpreted by the optical singularity of the Poynting vector. The negative nonconservative pulling force originates from the transfer of the azimuthal Poynting vector to the longitudinal component partly owing to the presence of a scatterer. The separatrice pattern and singularity shifts of the Poynting vector unanimously exhibit a differentiable near-field distribution in the presence of optical pulling force. A new method is established to calculate the near-field optical force using the differential Poynting vector in the far field. The results obtained provide a clear physical interpretation of the light–matter interaction and manifest the significance of singular optics in manipulating objects.

ORIGINAL PAPER
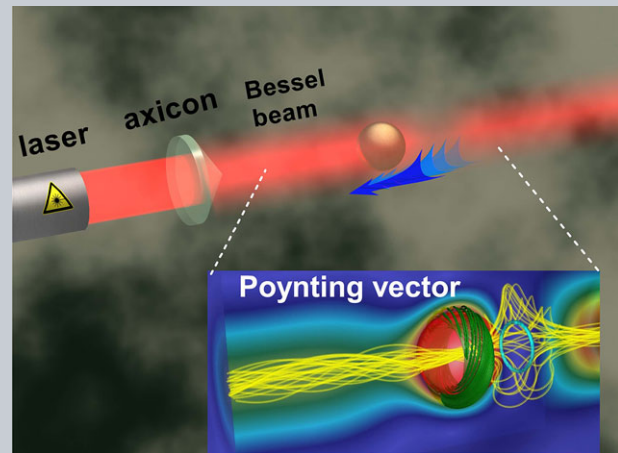
Unveiling the correlation between non-diffracting tractor beam and its singularity in Poynting vector

Dongliang Gao[1,2], Andrey Novitsky[3], Tianhang Zhang[1,4], Fook Chiong Cheong[5], Lei Gao[2], Chwee Teck Lim[4,6], Boris Luk'yanchuk[7], and Cheng-Wei Qiu[1,4,*]

1. Introduction

Along with optical manipulation arising in electromagnetic fields with a gradient [1–3], tractor beams [4–11] have been showing unprecedented phenomena that once only existed in science fiction. Unlike conventional optical tweezers which rely on adjusting the positions of intensity gradients to move objects, tractor beams can exert non-conservative pulling forces on particles by continuously dragging them towards the beam sources. Recently, experiments on tractor beams have been demonstrated using various structured beams. Stable trapping and bidirectional transport were achieved by systematically changing the relative phase of two co-propagating Bessel beams [12, 13]. Lee et al. [14] reported the first experimental observation of a functioning tractor beam by reversing the helical pitches of an optical solenoid beam. In addition to optical transport, binding forces from tractor beams can also be used to maneuver the behaviors of self-arranged structures [15,16].

As found from many theoretical and experimental studies, non-diffracting beams [17–19] are promising candidates for realizing tractor beams due to their unique properties of maintaining both intensity and spatial extent in the direction of propagation. Such tractor beams can exert pulling forces on a particle, which can be explained by using the law of momentum conservation, i.e. when the forward scattering exceeds the backward one, the particle experiences a backward-directed momentum [20]. In this paper, the pulling effect is explained from another perspective by employing singular optics. It is shown that the optical singularity of the Poynting vector around the scatterer helps one to understand the behaviors of the proposed tractor beams [8–11, 14].

Singular optics became a new branch of modern optical science nearly four decades ago, starting with the study of wave front dislocations by Nye and Berry [21]. Optical singularity is a ubiquitous phenomenon in the interference of multiple waves, e.g. between an incident wave and

[1] Department of Electrical and Computer Engineering, National University of Singapore, 4 Engineering Drive 3, Singapore 117576, Republic of Singapore

[2] College of Physics, Optoelectronics and Energy & Collaborative Innovation Center of Suzhou Nano Science and Technology, Soochow University, Suzhou 215006, China

[3] Department of Theoretical Physics and Astrophysics, Belarusian State University, Nezavisimosti Avenue 4, 220030 Minsk, Belarus

[4] NUS Graduate School for Integrative Sciences and Engineering, National University of Singapore, 28 Medical Drive, Singapore 117456, Republic of Singapore

[5] Mechanobiology Institute National University of Singapore, 5A Engineering Drive 1, Singapore 117411, Republic of Singapore

[6] Department of Mechanical Engineering, National University of Singapore, 9 Engineering Drive 1, Singapore 117576, Republic of Singapore

[7] Data Storage Institute, Agency of Science, Technology and Research, 5 Engineering Drive 1, Singapore 117608, Republic of Singapore

*Corresponding author: e-mail: eleqc@nus.edu.sg

reflected [22] or scattered light [23]. Phase singularities in electromagnetic fields give an additional insight into propagation and interaction of electromagnetic waves. Latest research, such as that concerning the quantum entanglement of linked phase singularities [24], spin–orbit interaction phenomena within vortex beams [25], and polarization singularities in vector beam fields [26, 27], has greatly expanded the sphere of modern optics. According to the condition for eigenvalues of the stability matrix [28, 29], the singular points in a vector field, such as the Poynting vector field, can be classified as node, saddle, vortex, and focus [30], which are accompanied by the concept of wave dislocation of wave interference [21]. Those singular points of the Poynting vector can be created, moved, and annihilated [31, 32], revealing a change of energy flow in the near field.

Being a basic concept in electrodynamics, the Poynting vector plays a pivotal role in understanding the physics of light scattering [32, 33] and optical force [34, 35]. The Poynting vector $\mathbf{S}$ in a vacuum can be associated with the linear momentum as $\mathbf{G} = (1/c^2) \int \mathbf{S} dV$ (where c is the speed of light). Based on the Poynting theorem, interpreting the Poynting vector as the energy flux density can be generalized for nonlinear and spatial dispersive media [36]. In this paper, we relate the optical force of a non-diffracting beam with the Poynting vector and describe it in terms of optical singularity. The optical pulling force can be realized by manipulating the distribution of singular points around the particle. Meanwhile, the interference of transverse electric (TE) and transverse magnetic (TM) Bessel beams can generate both positive and negative longitudinal components of the Poynting vector [37]. We discuss below the correlation between near-field (within one wavelength from the particle's surface) and far-field Poynting vectors and we elaborate the origin of the pulling force as a consequence of the specific energy flow.

2. Methods, results, and discussion

2.1. Calculating optical forces for nonparaxial Bessel beam

Non-diffracting beams or diffraction-free beams are structured beams that suppress the universal phenomena of diffraction and keep their cross-sectional intensity invariant during propagation [19]. They exist in various kinds of modes, Bessel, Airy, and Mathieu modes [18,38–40], with the Bessel beam being extensively studied. In this paper, we use the model of the nonparaxial Bessel beam (see details in Refs. [9, 10, 37] and similar models [15, 18, 41, 42]) with the electric field $\mathbf{E}(\mathbf{r}) = \exp(im\varphi + i\beta k_0 z)(c_1 \mathbf{E}_{TE}(r) + c_2 \mathbf{E}_{TM}(r))$, where m is the beam order and c_1 and c_2 are the complex amplitudes of the TE and TM constituents of the light beam. The normalized longitudinal wavenumber β and the transverse wavenumber q can be expressed as $\beta = \cos\alpha$ and $q = \sqrt{1 - \beta^2}$, respectively, with α being an angle between the wave vectors of partial

plane waves and the optical axis z. Thus, the longitudinal component of the optical force in dipole approximation, exerted by the non-diffracting beam, can be derived from Eq. (2) in Ref. [43] (a detailed derivation is presented in the Supporting Information, Section 1):

$$\langle F_z \rangle = \frac{k_0 \beta}{2} \left(\text{Im}(\alpha_e)|\mathbf{E}|^2 + \text{Im}(\alpha_m)|\mathbf{B}|^2 \right)$$
$$- \frac{k_0^4}{12\pi\varepsilon_0 c} \text{Re}(\alpha_e \alpha_m^* (\mathbf{E} \times \mathbf{B}^*)_z), \quad (1)$$

where $k_0 = \omega/c$ is the wavenumber in vacuum, ω is the angular frequency, and c is the speed of light. Electric and magnetic dipole moments linearly depend on the fields, i.e. $\mathbf{p} = \alpha_e \mathbf{E}$ and $\mathbf{m} = \alpha_m \mathbf{B}$. In general, electric and magnetic polarizabilities $\alpha_{e,m}$ of a spherical particle are expressed in terms of the sum of Mie coefficients a_v and b_v ($v = 1$ for the dipole, $v = 2$ for the quadrupole, etc.) [44]. When the higher-order multipole terms ($v = 2, 3, \ldots$) are much smaller than the dipole terms, the spherical particle can be approximated as a dipole, i.e. $\alpha_e = i6\pi a_1 \varepsilon_0 k_0^{-3}$ and $\alpha_m = i6\pi b_1 \mu_0^{-1} k_0^{-3}$. The first-order Mie coefficients have the following forms [44]:

$$a_1 = \frac{n^2 j_1(nx)(x j_1(x))' - \mu j_1(x)(nx j_1(nx))'}{n^2 j_1(nx)(x h_1^{(1)}(x))' - \mu h_1^{(1)}(x)(nx j_1(nx))'}, \quad (2)$$

$$b_1 = \frac{\mu j_1(nx)(x j_1(x))' - j_1(x)(nx j_1(nx))'}{\mu j_1(nx)(x h_1^{(1)}(x))' - h_1^{(1)}(x)(nx j_1(nx))'}, \quad (3)$$

where $x = k_0 R$, R is the particle radius, n is the spherical particle refractive index, j_1 and $h_1^{(1)}$ are spherical Bessel and Hankel functions of the first order, and a prime means differentiation with respect to the argument.

The first two terms of Eq. (1), describing the radiation pressure of the bare dipoles, are positive for particles made of ordinary materials. They can be negative for exotic media, such as gain particles [45, 46]. The necessary condition for the pulling force is to ensure that the third term is negative (see further discussion in the Supporting Information, Section 1). By using a nonparaxial Bessel beam, the small longitudinal wavenumber β can reduce the positive radiation pressure. Meanwhile, the corresponding transverse wavenumber q is relatively large, which could provide the prerequisite of transferring more azimuthal component of the Poynting vector to the transmitted longitudinal component. This results in even greater pulling force. This mechanism effectively enlarges forward momentum and gives an additional degree of freedom to manipulate the optical force through a non-diffracting beam.

Figure 1a clearly shows that there is a region of the radii of a nonmagnetic ($\mu = 1$) particle, $1 < k_0 R < 2$, where $\langle F_z \rangle$ is negative. The pulling force in this configuration is basically the result of dipole interaction. The force calculated using the dipole Mie coefficients is qualitatively correct for $k_0 R < 1.6$. The influence of higher-order moments comes into play only when the particle size is much
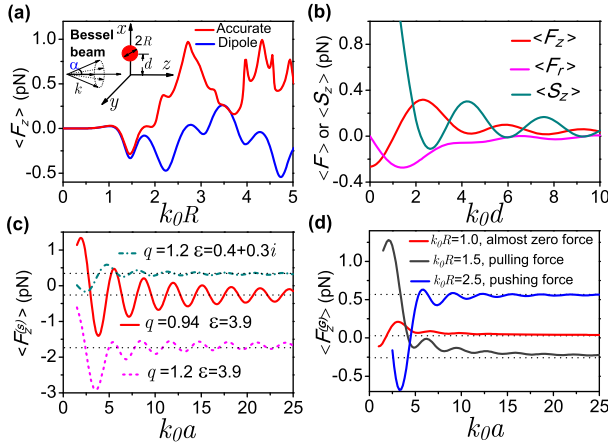
Figure 1 (a) Force of a spherical silica particle at the beam axis, i.e. $d = 0$. The inset is a sketch of a nonparaxial Bessel beam incident on a particle. (b) Force components and S_z as functions of particle position with respect to the beam axis $k_0 d$. (c) Poynting- and (d) field momentum-based forces taking asymptotic values (dotted lines) only for $a \to \infty$, where a is the radius of integrating surface. Default parameters: $\varepsilon = 3.9$, $\mu = 1$, $k_0 R = 1.5$, $m = 1$, $\alpha = 70°$, $c_1 = 1$, $c_2 = i$. The incident laser wavelength is set as 1064 nm and the intensity of the Bessel beam's center is normalized to 1 mW μm^{-2}.

larger. Moreover, Eq. (1) for the force is also valid when the dipole approximation holds. Therefore the pulling force in Fig. 1a can be simply explained by the interaction of the electric and magnetic dipoles (artificial magnetic dipole is discussed in Refs. [47–51]). In Fig. 1b we can observe the correlation between the Poynting vector S_z and the force $\langle F_z \rangle$ in agreement with Eq. (1). At the same time, the radial component of the force is directed towards the beam axis attracting the spheres therein.

It is of great importance to analyze larger particles beyond the dipolar approximation in terms of the total Poynting vector $\tilde{\mathbf{S}} = (1/2)\mathrm{Re}(\tilde{\mathbf{E}} \times \tilde{\mathbf{H}}^*)$, which can be related to the optical singularity. In this paper, the symbol ~ denotes total fields, i.e. the fields $\tilde{\mathbf{E}} = \mathbf{E} + \mathbf{E}_{sc}$ and $\tilde{\mathbf{H}} = \mathbf{H} + \mathbf{H}_{sc}$ are the sum of the incident and scattered fields. When the integration surface σ in $\langle \mathbf{F} \rangle = \int_\sigma (\mathbf{n} \cdot \hat{\mathbf{T}}) ds$ (with $\mathbf{n}$ being the normal direction to the particle surface and $\hat{\mathbf{T}} = (1/2)\mathrm{Re}[\varepsilon_0 \tilde{\mathbf{E}} \otimes \tilde{\mathbf{E}}^* + \mu_0 \tilde{\mathbf{H}} \otimes \tilde{\mathbf{H}}^* - (\varepsilon_0 |\tilde{\mathbf{E}}|^2 + \mu_0 |\tilde{\mathbf{H}}|^2)\hat{\mathbf{I}}/2]$, $\otimes$ denoting dyadic products and $\hat{\mathbf{I}}$ being the identity matrix) is taken at infinity, the scattered wave behaves like a spherical wave. The time-averaged Maxwell stress tensor can be simplified, and consequently the optical force takes the form $\langle \mathbf{F} \rangle = -(1/c)\int_{\sigma_\infty} \Delta \mathbf{S} ds$, where the Poynting vector difference is $\Delta \mathbf{S} = \tilde{\mathbf{S}} - \mathbf{S}$. Because scattered waves in the near field are not mere spherical waves, the formula $\langle \mathbf{F}^{(S)} \rangle = -(1/c)\int_\sigma \Delta \mathbf{S} ds$ is not valid for all spherical surfaces σ (integration spherical surface at radius a). Unfortunately, $\langle \mathbf{F}^{(S)} \rangle$ does not provide accurate information about the direction of the force. According to Fig. 1c, the "force" $\langle F_z^{(S)} \rangle$ oscillates between positive and

negative values and will be valid only at sufficiently large integration radius a.

By investigating the singularity distribution of Poynting vector difference $\Delta \mathbf{S}$, we can get better insight into the oscillatory behavior of $\langle F_z^{(S)} \rangle$. In the x–z plane, the Poynting vector lines can be described by the solutions of the dynamic differential equation $S_x dz = S_z dx$ [23, 52]. There are two kinds of singular points in this optical dynamic system: vortex (for $u > 0$) and saddle (for $u < 0$), where $u = \frac{\partial S_x}{\partial x}\frac{\partial S_z}{\partial z} - \frac{\partial S_x}{\partial z}\frac{\partial S_z}{\partial x}$ [28–30]. Alternatively, the type of singular points can be numerically characterized by the pattern of flow lines. In Fig. 2, we separate the domains of positive and negative values of $F_z^{(S)}$ with circles. The singular points ($\tilde{S}_x = S_x$, $\tilde{S}_z = S_z$) in these domains can significantly influence the behavior of $F_z^{(S)}$ because they change the direction of $\Delta \mathbf{S}$. The stability of the singular points alternates for a particle with small radius R (Fig. 2a), where vortices and saddles can be associated with the negative and positive $F_z^{(S)}$, respectively. However, this is not a universal rule because it is violated when the singularities are located densely but irregularly for larger spheres (Fig. 2b,c). The singularities appear and disappear in pairs of stable and unstable points keeping the same Poincaré index. Importantly, the singular points change the direction of the Poynting vector lines and, therefore, change the sign of the "force" $F_z^{(S)}$.

As depicted in Fig. 2, the dynamics of Poynting vector singularities around the particle results in oscillation of $F_z^{(S)}$ in Fig. 1c. The periodicity of oscillation is determined by the transverse periodicity of the incident Bessel beam and, therefore, does not depend entirely on the parameters of the scattering particle. Evanescent waves (corresponding to the curves with $q > 1$ in Fig. 1c) take the correct sign of the resultant force.

The formula $\langle \mathbf{F} \rangle = -(1/c)\lim_{a\to\infty}\int_\sigma \Delta \mathbf{S} a^2 ds$, with the integrand $a^2 \Delta \mathbf{S}(a)$ independent of the radial position r, can be rewritten as an average over the radial coordinate $\langle \mathbf{F} \rangle = -\lim_{L\to\infty}(1/cL)\int_R^{R+L}\int_\sigma \Delta \mathbf{S} a^2 dr ds$. One can divide the integral into two parts: $[R, R']$ and $[R', R+L]$, in which R' is a large number. The integral within $[R, R']$ is finite, and it vanishes when being divided by an infinitely large value L. With R' being large enough, one can write $a^2 \Delta \mathbf{S}(a) \approx r^2 \Delta \mathbf{S}(r)$. Then previous $\langle \mathbf{F} \rangle$ can be rewritten over the whole region $[R, R+L]$ as the following expression:

$$\langle \mathbf{F} \rangle = -\lim_{L\to\infty}\frac{1}{cL}\int_R^{R+L}\int_\sigma \Delta \mathbf{S}(\mathbf{r}) dV . \qquad (4)$$

After introducing the field momentum as $\mathbf{G} = (1/c^2)\int_R^\infty \int_\sigma \mathbf{S}(\mathbf{r}) dV$, the force takes a more significant meaning than it takes in terms of the Poynting vector. The force $\langle \mathbf{F} \rangle = \Delta \mathbf{G}/\Delta t$ is that of Newton's second law, where $\Delta \mathbf{G} = -(\tilde{\mathbf{G}} - \mathbf{G})$ is the momentum received by a particle during the time $\Delta t = L/c$ of the momentum transfer. Therefore, to ensure the pulling force is in the z direction, it is necessary to enhance the linear momentum of the field after scattering in the propagation direction. The force
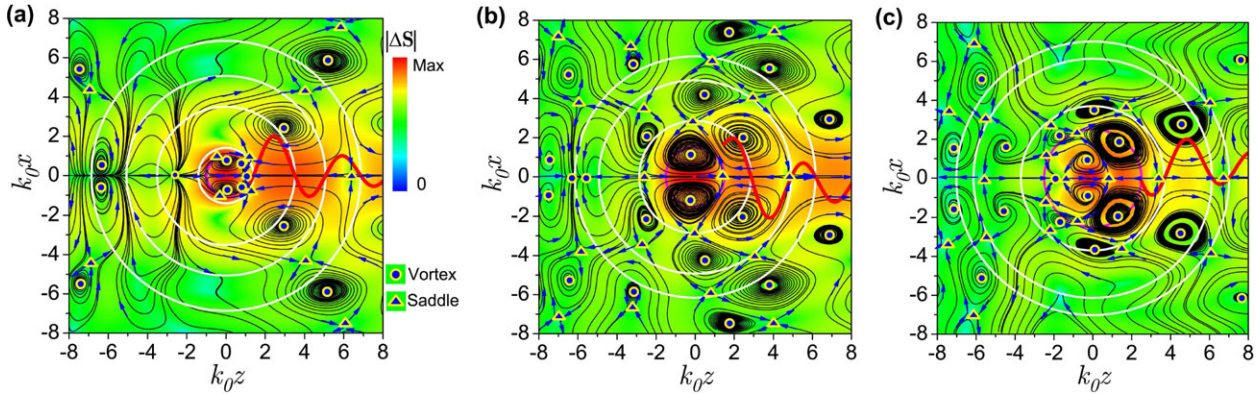
Figure 2 (color online). Distribution of $\triangle\mathbf{S}$ for a particle at the beam axis $d = 0$ for various radii of the sphere: (a) $k_0 R = 1.0$, (b) $k_0 R = 1.5$, and (c) $k_0 R = 2.5$. Red curves represent $F_z^{(S)}$, while the white circles pass through the zeros of $F_z^{(S)}$. The pink circles represent silica particles. Wave propagates from left- to right-hand side. Parameters: $\varepsilon = 3.9$, $\mu = 1$, $m = 1$, $\alpha = 70°$, $c_1 = 1$, $c_2 = i$.

calculated as $\langle\mathbf{F}^{(G)}\rangle = -(1/c(a - R))\int_R^a \int_\sigma \Delta\mathbf{S}(\mathbf{r})\mathrm{d}V$ converges to the asymptotic value for large integration radius a (see Fig. 1d), and the correct sign of the force can be derived faster than in Fig. 1c.

2.2. Explanations of nonconservative pulling force with singular optics

In what follows, we choose three typical situations (almost zero force but still pushing in Fig. 3a,b, pulling force in Fig. 3c,d, and pushing force in Fig. 3e,f) to illustrate the relations between the near-field singular points and optical force. For a relatively small dielectric sphere, the pairs of saddle–vortex Poynting vector singularities appear far away from the particle, as shown in Fig. 3a. The Bessel beam does not interact significantly with the particle and basically maintains its profile after transmission through the particle. Since there is a considerable amount of scattered light in the backward direction, the momentum of the incident beam is larger than that of the transmitted one, prompting a small pushing force. By increasing the size of the dielectric sphere, the energy flow of the Bessel beam is greatly twisted around the particle. Meanwhile, new singular points are created and move towards the particle, which alters the energy flow at those regions.

In the vicinity of the particle, six pairs of saddle–vortex singularities redirect the central energy channel through the particle (see Fig. 3c). For example, taking the middle two saddle–vortex pairs (marked 2 and highlighted in cyan), the light passes through the saddle points, makes a loop around the vortex points, comes back to the saddle points, and travels along the propagation direction. Energy flows, from the first ring of the non-diffracting Bessel beam, are captured by the particle while rotating around vortex points. Their combined effect can be visualized: the saddle points "grab" the light from the surrounding and the vortex points "store" the light within the rotation area. The other four pairs of saddle–vortex points (marked 1 and 3)

behave similarly. These singular points attract, guide, and focus the energy flow into the center of the particle. This kind of mechanism is similar to the phenomenon whereby fish in fluid flow capture energy from surrounding vortices to reduce muscle activity [53]. By further increasing the particle size, the crucial saddle–vortex points 3 are annihilated and the energy-capturing mechanism is undermined. Although other vortex–saddle points can still redirect energy flow from the second ring of the Bessel beam, the strength is much weaker and far away from the particle (Fig. 3e). So the pulling force decreases from maximum to zero and then becomes a pushing force again.

It is pertinent to show the three-dimensional distribution of Poynting vectors in the presence of vortices and scatterer, as this reveals the interaction between the singularity and the energy flow and helps in understanding how their combined effect facilitates the pulling force. Figure 3d presents, for the very first time, the singular optics of the tractor beam and the intriguing energy flow in the context of optical pulling force. One can clearly see that energy flow streamlines are strongly twisted around particles. These nonuniform helical distributions of the field can induce additional spin curl forces [54], which can be exploited to control objects near the particle. The vortex circle [55] in the vicinity of the particle front (see Fig. 3d) can redirect energy flows to the forward direction. By enlarging the particle size from $k_0 R = 1$ to $k_0 R = 2$, we find the position and size of the vortex circle play a vital role in realizing pulling force. As the vortex circle approaches the particle (the circle's radius also decreases simultaneously), its ability to focus energy is enhanced and the strength of the pulling force increases correspondingly. After the vortex circle disappears, the pulling force becomes weaker and eventually turns into a pushing force.

The subsequent discussion will elucidate the momentum enhancement in Poynting vector $\tilde{S}_z$. For a plane wave, the straight lines of the Poynting vector will be diverted away from the propagation direction due to the scattering of particles. Therefore, the transmitted Poynting vector in the propagation direction is always less than that of the
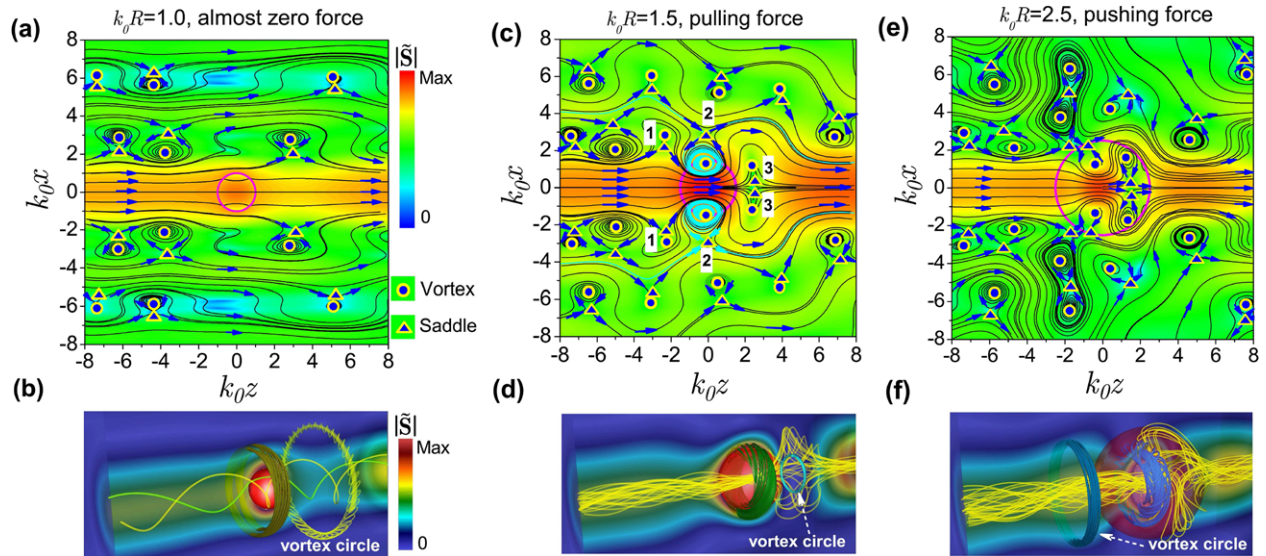
Figure 3 (color online). Two-dimensional distributions of the Poynting vector $\tilde{\mathbf{S}}$ (in a.u.) for various radii of the sphere: (a) $k_0R = 1.0$, (c) $k_0R = 1.5$, and (e) $k_0R = 2.5$. (b, d, f) The corresponding three dimensional distributions of $\tilde{\mathbf{S}}$. Some vortex points in two dimensions may form vortex circles in three dimensions. The pink circles in the two-dimensional images and red spheres in three-dimensional images represent the silica particles. Note that the colors of streamlines do not correspond to the color bar. Different colors are used to visually differentiate these Poynting vector lines at different regions. The streamlines in (b), (d), and (f) only demonstrate the trajectory of a few representative Poynting distributions showing the singular optics behavior. Parameters: $\varepsilon = 3.9$, $\mu = 1$, $m = 1$, $\alpha = 70°$, $c_1 = 1$, $c_2 = i$.

initial wave. According to momentum conservation, the plane wave always pushes the particle. The force could be pulling if the transmitted momentum is increased by using gain media [45]. This pulling force can be understood from stimulated emission of new photons initiated by the external pumping. In contrast, it is counterintuitive to "amplify" the S_z component in a totally passive system. Fortunately, we find that it is possible to transfer azimuthal S_φ to longitudinal S_z, which can be amplified via a passive light–matter scattering setup.

An incident non-diffracting Bessel beam has both longitudinal S_z and azimuthal S_φ components of the Poynting vector $\mathbf{S}(\mathbf{r}) = (0, S_\varphi, S_z)$ [37]. As a result of the scattering process, the longitudinal component of the total Poynting vector takes the form $\tilde{S}_z = M_1(\mathbf{r}, \mathbf{E}, \mathbf{H})S_\varphi + M_2(\mathbf{r}, \mathbf{E}, \mathbf{H})S_z$, where $M_{1,2}$ are two operators acting on the incident Poynting vector components. For paraxial beams ($S_\varphi \ll S_z$) and plane waves ($S_\varphi = 0$), the longitudinal component $\tilde{S}_z$ cannot be enlarged or effectively controlled using S_φ. On the contrary, the nonparaxial beam stores much energy in the azimuthal Poynting component which can be effectively reallocated to the longitudinal component.

The mutual transformation between $\tilde{S}_\varphi$ and $\tilde{S}_z$ is illustrated in Fig. 4. Large azimuthal component S_φ (blue lines) is associated with two series of saddle–vortex pairs that are marked with Arabic numerals (between the first ring and the beam center) and Roman numerals (between the first ring and the second ring) in Fig. 4b. Small particles (Fig. 4a) slightly disturb the incident Bessel beam. For larger particles shown in Fig. 4b, the azimuthal component of the

Poynting vector is captured inside the particle, while the incident S_z from the first ring of the Bessel beam contributes to the amplification of the total Poynting vector component $\tilde{S}_z$. The singular points (marked 5) prevent the flow of the azimuthal component and redirect the flow of the longitudinal component. The singularities I–V operate similarly for the outer rings of the Bessel beam. Eventually, the extra energy flux that originates in the transformation from azimuthal component S_φ to longitudinal component S_z drags the particle towards the light source. Larger particles lose a singular point on the right-hand side of it and corresponding mutual transformation is not carried out effectively. Note that the above explanation of momentum enhancement is not limited to the nonparaxial Bessel beams of first order ($m = 1$). It is also valid for other orders, such as the zero-order nonparaxial Bessel beams considered in Chen et al. [9]. However, the zero-order Bessel beam with $S_\varphi = 0$ was used as an example of nonparaxial Bessel beams in their work, and hence there was no contribution from the transfer of azimuthal to longitudinal components. This explains why the magnitude of the pulling force by beams with $S_\varphi = 0$ is much weaker than by beams with $S_\varphi \neq 0$. Hence, Bessel beams with considerably large azimuthal component S_φ are more favorable for acting as tractor beams.

The far-field scattering is in accordance with near-field singular points. For a tiny particle, singular points exist only in the region of small incident energy flux density, providing small perturbations due to scattering. The scattering becomes stronger and the singular points marked 3 in Fig. 3c move to the intense main lobe of the incident Bessel beam. This means that the magnitude of the scattered
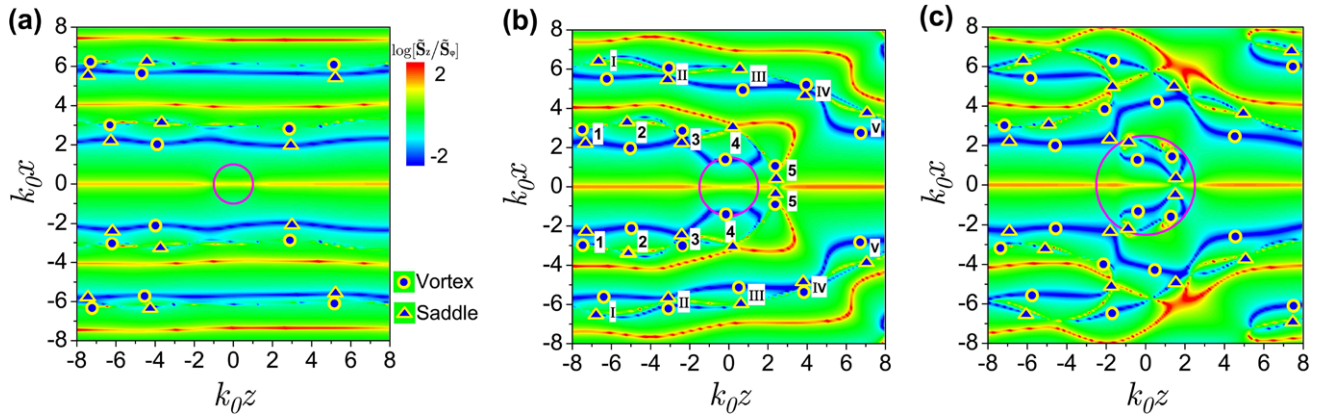
Figure 4 (color online). The transformation of longitudinal and azimuthal components of the Poynting vector: (a) $k_0 R = 1.0$, (b) $k_0 R = 1.5$, and (c) $k_0 R = 2.5$. The color represents the value of $\log[\tilde{S}_z/\tilde{S}_\varphi]$. The Bessel beam propagates in vacuum without transformation between S_φ and S_z. Interacting with a particle, these components are coupled and transfer one to another. A considerable amount of the azimuthal component of the Poynting vector should be transferred to the longitudinal component to ensure the backward optical force ($k_0 R = 1.5$).
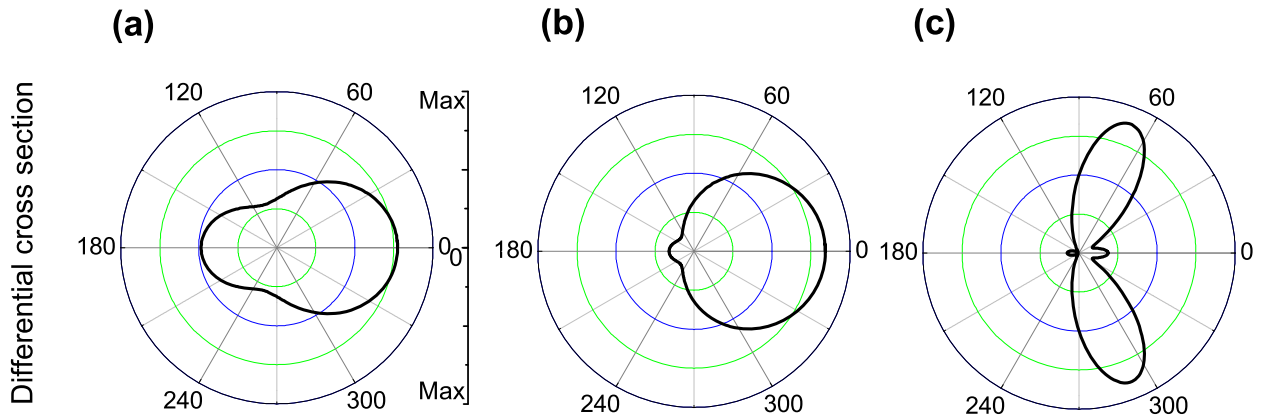
Figure 5 (color online). Far-field scattering diagrams for particles: (a) $k_0 R = 1.0$, (b) $k_0 R = 1.5$, and (c) $k_0 R = 2.5$. The other parameters are the same as in Fig. 3.

field in the forward direction is comparable with that of the incident field. When the forward scattering is significant enough (Fig. 5b), the optical force becomes pulling. This occurs when the singularities in front of the object drift to the geometrical shadowed region. In this case, the particle effectively transmits the energy flux through it due to the singular points denoted 2 in Fig. 3c, providing strong forward scattering. The increase of the particle radius R moves singularities 3 towards the optical axis and simultaneously towards the particle interface. When the singularities penetrate into the sphere, the scattering no longer focuses on the forward direction (see Fig. 5c), and thus the force becomes pushing again.

3. Conclusions and outlook

In conclusion, optical pulling force is realized owing to an increase of the field momentum. The necessary condition of pulling force exerted on small dielectric objects is a large

positive longitudinal Poynting vector at the particle center. Backward force on larger dielectric particles is achieved due to the emergence of singular points in the forward direction. These singular points of the Poynting vector result in large forward scattering and serve to redirect the stored angular momentum S_φ into linear momentum S_z. We extended the far-field calculations of the optical force, $\langle \mathbf{F} \rangle = -(1/c) \int_{\sigma_\infty} (\tilde{\mathbf{S}} - \mathbf{S}) ds$, to the near field. In this case, the calculated forces show oscillating behavior due to the singular points in the near field and eventually tend to the asymptotic value in the far field.

The insight into the optical pulling force is not only helpful in understanding light–matter interactions, but also provides new principles for the design of intriguing classes of tractor beams. The optical singularity can be designed to mold the energy flow in optical systems, which could extend the manipulation from trapping to rotating and sorting. For instance, non-diffracting tractor beams, carrying certain angular momentum, will rotate chiral particles with different handedness in opposite directions.

This rotational effect can be exploited to sort left-handed and right-handed DNA molecules. Meanwhile, apart from light interaction with matter associated with linear momentum, comprehensive investigation is required for angular momentum as well. Singular optics could be an alternative powerful tool for revealing the intrinsic mechanism of exotic phenomena and very fundamental wave properties in the near field of objects, e.g. counterintuitive left-handed optical torque which has a direction opposite to that of the optical angular momentum of incident light [56].

References

[1] Y. Roichman, B. Sun, Y. Roichman, J. Amato-Grill, and D. G. Grier, Phys. Rev. Lett. **100**, 013602 (2008).

[2] V. Ginis, P. Tassin, C. M. Soukoulis, and I. Veretennicoff, Phys. Rev. Lett. **110**, 057401 (2013).

[3] R. Quidant and C. Girard, Laser Photonics Rev. **2**, 47 (2008).

[4] S. Sukhov and A. Dogariu, Phys. Rev. Lett. **107**, 203602 (2011).

[5] S. Sukhov and A. Dogariu, Opt. Lett. **35**, 3847 (2010).

[6] M. Duocastella and C. B. Arnold, Laser Photonics Rev. **6**, 607 (2012).

[7] M. Woerdemann, C. Alpmann, M. Esseling, and C. Denz, Laser Photonics Rev. **7**, 839 (2013).

[8] J. J. Sáenz, Nat. Photonics **5**, 514 (2011).

[9] J. Chen, J. Ng, Z. Lin, and C. T. Chan, Nat. Photonics **5**, 531 (2011).

[10] A. Novitsky, C. W. Qiu, and H. Wang, Phys. Rev. Lett. **107**, 203601 (2011).

[11] A. Novitsky, C. W. Qiu, and A. Lavrinenko, Phys. Rev. Lett. **109**, 023902 (2012).

[12] T. Čižmár, V. Kollárová, Z. Bouchal, and P. Zemánek, New J. Phys. **8**, 43 (2006).

[13] D. B. Ruffner and D. G. Grier, Phys. Rev. Lett. **109**, 163903 (2012).

[14] S. H. Lee, Y. Roichman, and D. G. Grier, Opt. Express **18**, 6988 (2010).

[15] V. Karásek, T. Čižmár, O. Brzobohatý, and P. Zemánek, Phys. Rev. Lett. **101**, 143601 (2008).

[16] O. Brzobohatý, V. Karásek, M. Šiler, L. Chvátal, T. Čižmár, and P. Zemánek, Nat. Photonics **7**, 123 (2013).

[17] J. Durnin, J. Opt. Soc. Am. A **4**, 651 (1987).

[18] J. Durnin, J. J. Miceli, and J. Eberly , Phys. Rev. Lett. **58**, 1499 (1987).

[19] M. Mazilu, D. J. Stevenson, F. Gunn-Moore, and K. Dholakia, Laser Photonics Rev. **4**, 529 (2010).

[20] P. L. Marston, J. Acoust. Soc. Am. **120**, 3518 (2006).

[21] J. F. Nye and M. V. Berry, Proc. R. Soc. Lond. A **336**, 165 (1974).

[22] W. Braunbek and G. Laukien, Optik **9**, 174 (1952).

[23] Z. B. Wang, B. S. Luk'yanchuk, M. H. Hong, Y. Lin, and T. C. Chong, Phys. Rev. B **70**, 035418 (2004).

[24] J. Romero, J. Leach, B. Jack, M. R. Dennis, S. Franke-Arnold, S. M. Barnett, and M. J. Padgett, Phys. Rev. Lett. **106**, 100407 (2011).

[25] K. Y. Bliokh, M. R. Dennis, and F. Nori, Phys. Rev. Lett. **107**, 174802 (2011).

[26] F. Flossmann, U. T. Schwarz, M. Maier, and M. R. Dennis, Phys. Rev. Lett. **95**, 253901 (2005).

[27] F. Flossmann, K. O'Holleran, M. R. Dennis, and M. J. Padgett, Phys. Rev. Lett. **100**, 203902 (2008).

[28] A. A. Andronov, A. A. Vitt, and S. E. Khaikin, Theory of Oscillators (Dover, New York, 1987).

[29] G. A. Korn and T. M. Korn, Mathematical Handbook for Scientists and Engineers (McGraw-Hill, New York, 1961).

[30] A. Bekshaev, K. Y. Bliokh, and M. Soskin, J. Opt. **13**, 053001 (2011).

[31] H. F. Schouten, T. D. Visser, and D. Lenstra, J. Opt. B **6**, S404 (2004).

[32] M. I. Tribelsky and B. S. Luk'yanchuk, Phys. Rev. Lett. **97**, 263902 (2006).

[33] B. S. Luk'yanchuk, M. I. Tribelsky, V. Ternovsky, Z. B. Wang, M. H. Hong, L. P. Shi, and T. C. Chong, J. Opt. A **9**, S294 (2007).

[34] A. Ashkin, Phys. Rev. Lett. **24**, 156 (1970).

[35] D. G. Grier, Nature **424**, 810 (2003).

[36] D. F. Nelson, Phys. Rev. Lett. **76**, 4713 (1996).

[37] A. V. Novitsky and D .V. Novitsky, J. Opt. Soc. Am. A **24**, 2844 (2007).

[38] M. Berry and N. Balazs, Am. J. Phys. **47**, 264 (1979).

[39] J. C. Gutiérrez-Vega, M. D. Iturbe-Castillo, and S. Chávez-Cerda, Opt. Lett. **25**, 1493 (2000).

[40] G. A. Siviloglou, J. Broky, A. Dogariu, and D. N. Christodoulides, Phys. Rev. Lett. **99**, 213901 (2007).

[41] W. X. Cong, N. X. Chen, and B. Y. Gu, J. Opt. Soc. Am. A **15**, 2362 (1998).

[42] D. McGloin and K. Dholakia, Contemp. Phys. **46**, 15 (2005).

[43] M. Nieto-Vesperinas, J. J. Sáenz, R. Gómez-Medina, and L. Chantada, Opt. Express **18**, 11428 (2010).

[44] C. F. Bohren and D. R. Huffman, Absorption and Scattering of Light by Small Particles (Wiley, New York, 1998).

[45] A. Mizrahi and Y. Fainman, Opt. Lett. **35**, 3405 (2010).

[46] K. J. Webb and Shivanand, Phys. Rev. E **84**, 057602 (2011).

[47] C. W. Qiu and L. Gao, J. Opt. Soc. Am. B **25**, 1728 (2008).

[48] A. B. Evlyukhin, C. Reinhardt, A. Seidel, B. S. Luk'yanchuk, and B. N. Chichkov, Phys. Rev. B **82**, 045404 (2010).

[49] A. Garcia-Etxarri, R. Gomez-Medina, L. S. Froufe-Perez, C. Lopez, L. Chantada, F. Scheffold, J. Aizpurua, M.

Nieto-Vesperinas, and J. J. Saenz, Opt. Express **19**, 4815 (2011).

[50] M. Nieto-Vesperinas, R. Gómez-Medina, and J. J. Sáenz, J. Opt. Soc. Am. A **28**, 54 (2011).

[51] A. I. Kuznetsov, A. E. Miroshnichenko, Y. H. Fu, J. Zhang, and B. Luk'yanchuk, Sci. Rep. **2**, 492 (2012).

[52] B. S. Luk'yanchuk and V. Ternovsky, Phys. Rev. B **73**, 235432 (2006).

[53] J. Liao, D. Beal, G. Lauder, and M. Triantafyllou, Science **302**, 1566 (2003).

[54] D. B. Ruffner and D. G. Grier, Phys. Rev. Lett. **108**, 173602 (2012).

[55] S. Franke-Arnold, L. Allen, and M. Padgett, Laser Photonics Rev. **2**, 299 (2008).

[56] D. Hakobyan and E. Brasselet, Nat. Photonics **8**, 610 (2014).

Supporting Information

Additional supporting information may be found in the online version of this article at the publisher's website.